AMERICAN SOCIETY FOR MICROBIOLOGY | Journal of Virology®

VIRUS-CELL INTERACTIONS

Epstein-Barr Virus Lytic Replication Induces ACE2 Expression and Enhances SARS-CoV-2 Pseudotyped Virus Entry in Epithelial Cells

Dinesh Verma,[a] Trenton Mel Church,[a] Sankar Swaminathan[a,b]

[a]Division of Infectious Diseases, Department of Medicine, University of Utah School of Medicine, Salt Lake City, Utah, USA
[b]Division of Microbiology and Immunology, Department of Pathology, University of Utah School of Medicine, Salt Lake City, Utah, USA

ABSTRACT Understanding factors that affect the infectivity of severe acute respiratory syndrome coronavirus 2 (SARS-CoV-2) is central to combatting coronavirus disease 2019 (COVID-19). The virus surface spike protein of SARS-CoV-2 mediates viral entry into cells by binding to the ACE2 receptor on epithelial cells and promoting fusion. We found that Epstein-Barr virus (EBV) induces ACE2 expression when it enters the lytic replicative cycle in epithelial cells. By using vesicular stomatitis virus (VSV) particles pseudotyped with the SARS-CoV-2 spike protein, we showed that lytic EBV replication enhances ACE2-dependent SARS-CoV-2 pseudovirus entry. We found that the ACE2 promoter contains response elements for Zta, an EBV transcriptional activator that is essential for EBV entry into the lytic cycle of replication. Zta preferentially acts on methylated promoters, allowing it to reactivate epigenetically silenced EBV promoters from latency. By using promoter assays, we showed that Zta directly activates methylated ACE2 promoters. Infection of normal oral keratinocytes with EBV leads to lytic replication in some of the infected cells, induces ACE2 expression, and enhances SARS-CoV-2 pseudovirus entry. These data suggest that subclinical EBV replication and lytic gene expression in epithelial cells, which is ubiquitous in the human population, may enhance the efficiency and extent of SARS-CoV-2 infection of epithelial cells by transcriptionally activating ACE2 and increasing its cell surface expression.

IMPORTANCE SARS-CoV-2, the coronavirus responsible for COVID-19, has caused a pandemic leading to millions of infections and deaths worldwide. Identifying the factors governing susceptibility to SARS-CoV-2 is important in order to develop strategies to prevent SARS-CoV-2 infection. We show that Epstein-Barr virus, which infects and persists in >90% of adult humans, increases susceptibility of epithelial cells to infection by SARS-CoV-2. EBV, when it reactivates from latency or infects epithelial cells, increases expression of ACE2, the cellular receptor for SARS-CoV-2, enhancing infection by SARS-CoV-2. Inhibiting EBV replication with antivirals may therefore decrease susceptibility to SARS-CoV-2 infection.

KEYWORDS Epstein-Barr virus, SARS-CoV-2, COVID-19, ACE2, transcription, epithelial cell

Cellular entry of severe acute respiratory syndrome coronavirus 2 (SARS-CoV-2), the agent of coronavirus disease 2019 (COVID-19), requires binding of the viral spike protein to the ACE2 receptor on epithelial cells followed by membrane fusion (1–3). Expression of the ACE2 receptor on the surface membranes of epithelial cells in the oropharynx, nasopharynx, and lower respiratory tract is therefore necessary for viral entry and affects the likelihood of SARS-CoV-2 infection (4, 5).

Epstein Barr virus (EBV) also gains entry into the host via the oropharyngeal epithelium and persistently infects >90% of the human population. EBV establishes latent infection in

Citation Verma D, Church TM, Swaminathan S. 2021. Epstein-Barr virus lytic replication induces ACE2 expression and enhances SARS-CoV-2 pseudotyped virus entry in epithelial cells. J Virol 95:e00192-21. https://doi.org/10.1128/JVI.00192-21.

Editor Richard M. Longnecker, Northwestern University

Address correspondence to Sankar Swaminathan, sankar.swaminathan@hsc.utah.edu.

Received 5 February 2021
Accepted 13 April 2021
Accepted manuscript posted online 14 April 2021
Published 10 June 2021

B lymphocytes and undergoes intermittent lytic reactivation, followed by lytic replication in epithelial cells, producing infectious virions, which are shed in the saliva (6, 7). EBV reactivation and lytic replication have pleiotropic effects on cellular gene expression (8). Because EBV infection is ubiquitous and replicates in oropharyngeal and nasopharyngeal epithelium, EBV reactivation may affect susceptibility to SARS-CoV-2 infection.

Here, we show that EBV reactivation and lytic gene expression lead to robust increases in ACE2 expression in epithelial cells infected with EBV. Further, such induction of ACE2 expression by EBV enhances specific ACE2-dependent entry of SARS-CoV-2 pseudotyped virions in EBV-infected cells. Expression of the EBV lytic transcriptional activator Zta enhances transcription from the ACE2 promoter, which contains Zta response elements. Zta preferentially activates methylated promoters, allowing it to activate epigenetically silenced genes. These data, taken together, indicate that subclinical EBV reactivation and lytic EBV gene expression may enhance the efficiency and extent of SARS-CoV-2 infection in humans.

RESULTS

EBV lytic replication induces ACE2 expression in epithelial cells. In our study of virus-host cell interactions during EBV lytic replication, we have analyzed the effects of EBV gene expression on host phenotype by deep sequencing of cellular RNAs before and during lytic EBV replication (9, 10). The epithelial cell system employs AGS cells derived from a human gastric carcinoma and infected by a recombinant Akata EBV strain which expresses GFP (10, 11). The EBV Zta transactivator protein encoded by the EBV BZLF1 gene is both necessary and sufficient for efficient initiation of the lytic cycle of EBV replication (12–14). We stably expressed an inducible Zta EBV gene in these cells by lentiviral transduction and established a cell line referred to as AGSiZ, which is highly permissive of lytic EBV replication when treated with doxycycline (10). Lytic gene expression, EBV DNA replication, and infectious virus production are robustly induced after Zta induction with doxycycline. To investigate the hypothesis that EBV reactivation may increase the risk or severity of SARS-CoV-2 disease, we examined the transcriptomic data for potential effects of EBV reactivation on cell molecules important for SARS-CoV-2 infection. EBV lytic replication induced distinct changes in cellular gene expression (Fig. 1A), and ACE2 was the 30th most upregulated cellular gene (138-fold) 24 h after EBV replication was induced. At 48 h, ACE2 was the 99th most induced gene (130-fold). To confirm this observation, we measured the relative amount of ACE-2 mRNA in cells that had been either mock induced or induced to enter lytic EBV replication. We found that ACE-2 mRNA levels increased over 500-fold as early as 24 h after lytic induction and remained elevated at 48 h (Fig. 1B). Notably, ACE2 expression was maximal at 24 h postinduction, a time at which early EBV lytic genes such as BMRF1 are highly expressed but which is prior to expression of late lytic EBV genes such as BcLF1 (Fig. 1B). Inhibition of EBV DNA replication with phosphonoacetic acid (PAA) did not affect ACE2 induction caused by EBV reactivation (Fig. 1C). Since DNA replication is required for efficient late EBV gene expression (9, 15), these data suggest that an early lytic EBV gene or cellular genes induced early during EBV reactivation enhance ACE2 expression.

ACE2 induction by EBV enhances entry by SARS-CoV-2-pseudotyped virus. To determine whether ACE2 induction by EBV led to a functional increase in ACE2 receptor activity, we adapted a pseudotyped vesicular stomatitis virus (VSV) system successfully used to study both Middle East respiratory syndrome (MERS) and SARS virus (16). Virions pseudotyped with the SARS-CoV-2 spike protein specifically bind ACE2 and mediate viral fusion with the cell membrane. Expression of SARS-CoV-2 S protein on the PV particle thus confers ACE2-dependent entry (17). A pseudotyped virus (PV) expressing the S (spike) protein of SARS-CoV-2 on its envelope was generated that also expresses firefly luciferase, allowing measurement of PV entry by luciferase assay. Infection of AGSiZ cells with SARS-CoV-2 PV was then performed after either mock induction or induction of EBV replication with doxycycline. Induction of EBV replication led to a 5- to 6-fold increase in SARS-CoV-2 PV entry (Fig. 2A). We also measured the entry of a VSV pseudotyped with Junin G protein in AGSiZ cells, and entry of the Junin

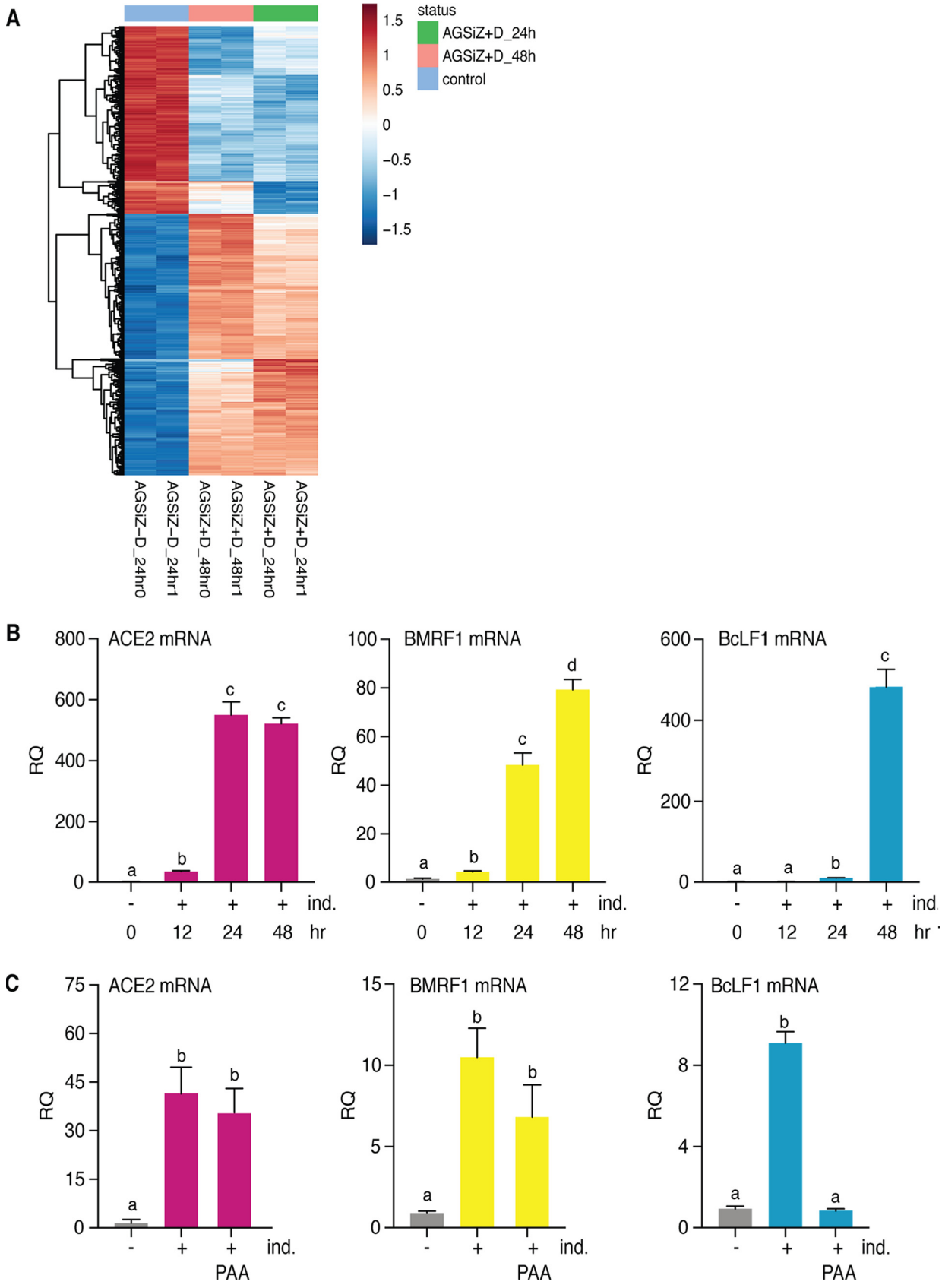

FIG 1 EBV lytic replication induces ACE2 expression. (A) Heat map of Z scores from normalized expression of cellular genes in AGSiZ cells after induction of EBV lytic replication (+D) compared to mock-induced cells (−D), 24 and 48 h after induction. ACE2 induction levels at each time

(Continued on next page)

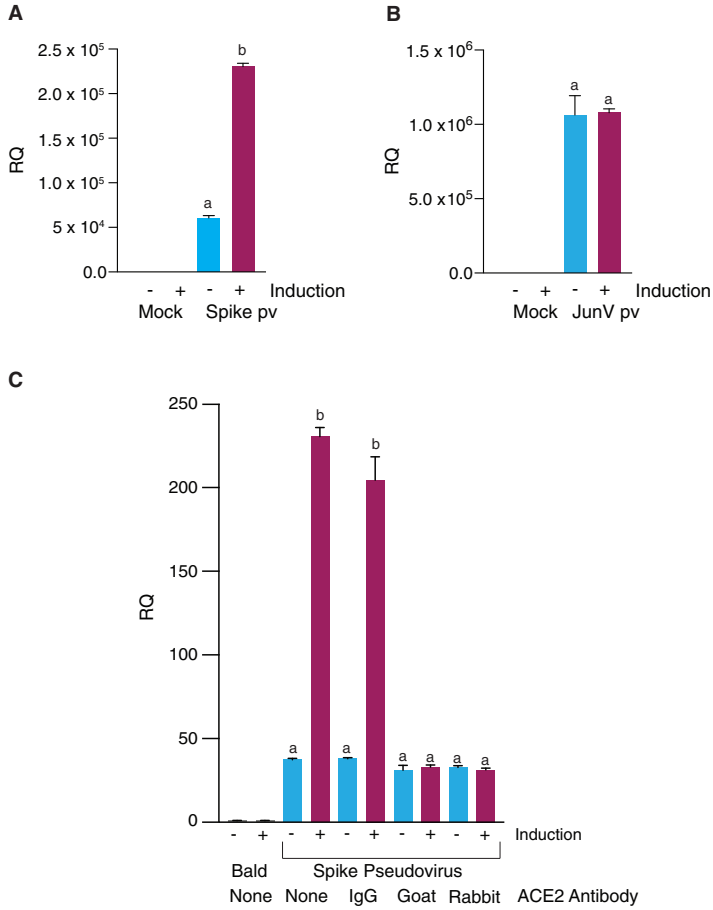

FIG 2 ACE2 dependent SARS-CoV-2 pseudovirus entry is enhanced by EBV reactivation. (A) SARS-CoV-2 pseudovirus (Spike PV) entry into AGSiZ cells was measured by luciferase assay and presented as a ratio of luciferase activity in each sample to that in mock-infected (RQ, relative quantity). AGSiZ cells were either induced or mock-induced to permit EBV lytic replication 48 h prior to infection with SARS-CoV-2 PV. (B) Infection of AGSiZ cells by Junin G protein pseudovirus (JunV PV) was measured by luciferase assay in cells. AGSiZ cells were either induced or mock induced prior to Junin G pseudovirus infection as for SARS-CoV-2 experiments. Protein lysates were harvested 24 h after PV infection and luciferase activity was measured. RQ, relative quantity. (C) Blockade of ACE-2 dependent entry was performed by preincubation of cells with either a rabbit or goat anti-ACE2 antibody for 1 h prior to infection with SARS-CoV-2 pseudovirus or with PV expressing no SARS-CoV-2 spike protein (bald). Mock antibody treatment was performed with rabbit IgG. A no-antibody control was also performed (None). Data are means and standard errors of the means for three independent experiments, with luciferase assays performed in technical triplicates. *P* values for each comparison are shown by letters above each bar. Nonsignificant differences are denoted with the same letter. Significant differences ($P < 0.0005$) are denoted by different letters.

G PV was not increased by EBV lytic replication, confirming that EBV lytic replication does not nonspecifically enhance ACE-independent pseudotyped virus entry (Fig. 2B). To confirm that the enhanced entry of SARS-CoV-2 PV was due to increased surface ACE2 expression on the surfaces of the EBV-infected cells, we asked whether ACE2 antibody would block

FIG 1 Legend (Continued)
point based on normalized read counts were 138-fold and 130-fold at 24 and 48 h after lytic induction, respectively. (B) Quantitative reverse transcription-PCR (RT-PCR) measurement of ACE2, early lytic EBV gene BMRF1, and late lytic gene BcLF1 mRNAs 12, 24, and 48 h after induction of EBV lytic replication. AGSiZ cells were either mock induced or induced with doxycycline, and RNA was isolated from each sample at the indicated times after induction. (C) Quantitative RT-PCR measurement of ACE2, early lytic EBV gene BMRF1, and late lytic gene BcLF1 mRNAs in the presence or absence of PAA added prior to induction of EBV replication. Data are means plus standard errors of the means for three independent experiments, with RT-PCR performed in technical triplicates. RQ, relative quantity; ind., induced to permit EBV lytic replication with doxycycline. *P* values for each comparison are shown by letters above each bar. For all comparisons, nonsignificant differences are denoted with the same letter and significant differences are denoted by different letters. All nonsignificant differences had *P* values of >0.5, and significant differences had *P* values of <0.0001, except that in panel B, for the 24-h versus 48-h BMRF1 comparison, *P* was <0.002, and in panel C, significant differences for ACE2 had a *P* value of <0.002 and nonsignificant differences for BMRF1 had a *P* value of >0.08.

SARS-CoV-2 PV entry. The increase in SARS-CoV-2 PV entry was blocked by two different antibodies against ACE2 but not by control antibody, demonstrating that the EBV-induced increase in SARS-CoV-2 PV infection was due to upregulated functional ACE2 receptor expression (Fig. 2C).

The ACE2 promoter is directly activated by EBV lytic replication. As described above, induction of ACE2 expression preceded late lytic gene expression and was not dependent on EBV DNA replication, which is required for EBV late gene expression (9, 15). The cascade of EBV lytic gene expression is initiated by a DNA-binding EBV transcriptional activator protein, Zta, which activates and synergizes with a second EBV transactivator, Rta, encoded by the EBV BRLF1 gene, to activate lytic EBV promoters (18–20). To investigate the possibility that one or both of these EBV proteins directly transactivate the ACE2 promoter, we constructed an ACE2 promoter reporter plasmid in which the luciferase gene was driven by the ACE2 promoter (ACE2p). To first validate the responsiveness of this reporter plasmid and confirm that EBV induction induces transcription from the ACE2 promoter, we transfected it into AGSiZ cells, which were then either induced or mock induced to permit EBV lytic cycle gene expression. Induction of EBV lytic cycle resulted in expression of both Zta and Rta and activation of ACE2 promoter-driven luciferase activity, indicating that EBV reactivation enhances ACE2 mRNA transcription (Fig. 3A).

The EBV transcriptional activator Zta preferentially acts on methylated ACE2 promoters. The ACE2p-luciferase plasmid was then transfected into EBV-negative AGS and 293T cells along with either Zta or Rta expression vectors or a combination of both Zta and Rta (Fig. 3B and C). The independent expression of each protein was confirmed by immunoblotting (Fig. 3B and C). In both cell types, the ACE2 promoter was transactivated by Rta but not by Zta.

Rta is a DNA-binding transcription factor that acts both by direct promoter binding to Rta response elements and by indirect modulation of cell signaling pathways (21–23). Inspection of the ACE2 promoter region did not reveal any canonical Rta response elements, suggesting that Rta might enhance ACE2 promoter by indirect mechanisms, as has been shown for Rta activation of the cellular genes c-*myc* and fatty acid synthase (24, 25). Inspection did, however, reveal that the ACE2 promoter contains three potential Zta response elements (ZREs) (26) (Fig. 4A). Although Zta did not transactivate the ACE2 promoter in cotransfection assays, Zta is preferentially active on methylated promoter regions, a property that facilitates reactivation of EBV lytic promoters epigenetically silenced by methylation (27–30). Since the transfected ACE2 reporter plasmids produced in bacteria would not be CpG methylated, unlike the cellular ACE2 promoter, it was possible that Zta was responsible for at least part of the induction of cellular ACE2 that occurred with EBV lytic replication.

To further investigate a role for Zta and the extent to which it could activate the ACE2 promoter, which is known to be epigenetically modified by methylation (31), we examined the effect of Zta on a methylated ACE2 promoter. We methylated the ACE2 promoter-luciferase expression vector *in vitro* by treatment with the M.SssI CpG methyltransferase and compared the effects of Zta and Rta on unmethylated and methylated ACE2 promoters (Fig. 4B). Upon methylation, the ACE2 promoter was strongly activated by Zta (85-fold), whereas the unmethylated promoter was not activated, as previously shown. Interestingly, the methylated promoter concomitantly became less responsive to Rta. These data suggested that Zta may play the primary role in transactivating ACE2 in EBV-infected cells upon entry into the lytic cycle from latency when both cellular and viral promoters are methylated. We therefore asked if depletion of Rta during lytic reactivation would significantly affect ACE2 induction by EBV. AGSiZ cells were first transfected with either a nontargeting control small interfering RNA (siRNA) or an Rta-specific siRNA. Rta depletion was confirmed by immunoblotting, and ACE2 induction was measured by qPCR. As shown in Fig. 4C, Rta depletion did not have a significant effect on ACE2 induction, indicating that Zta is the primary driver of ACE2 induction in EBV-infected cells, although other EBV genes may also play a role.

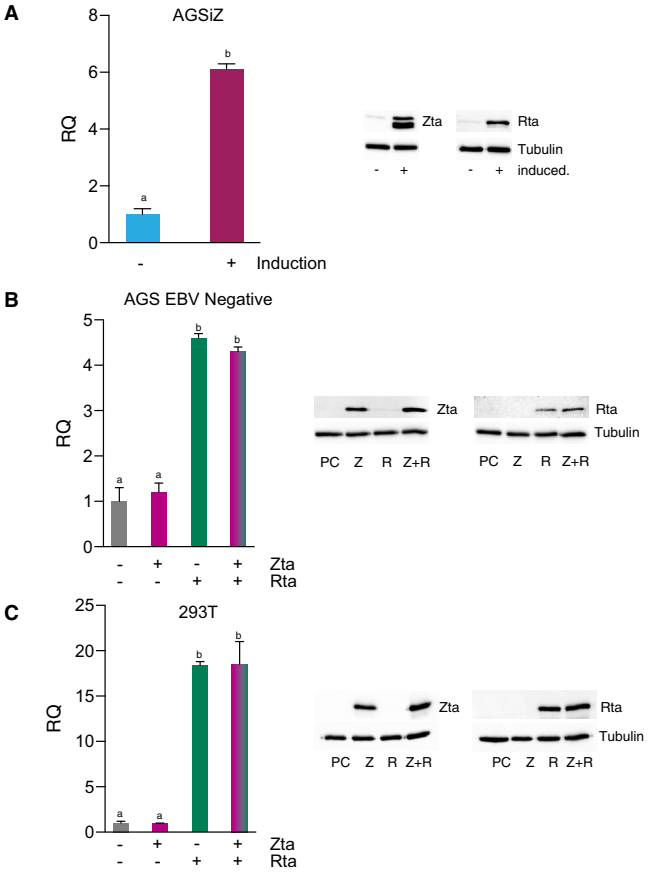

FIG 3 Effect of EBV transcriptional activators Zta and Rta on transcription from the ACE2 promoter. (A) An ACE2 promoter-driven luciferase reporter plasmid was transfected into EBV-positive AGSiZ cells 24 h after either induction or mock induction of EBV replication. Luciferase activity was measured 24 h after transfection and calculated as the ratio of signal in induced versus uninduced cells (RQ, relative quantity). Each transfection was performed in triplicate, and each lysate was assayed in technical triplicates. Protein expression of Zta and Rta after induction measured by immunoblotting is shown on the right, with tubulin as a loading control. (B) EBV-negative AGS cells were cotransfected with the ACE2-luciferase reporter plasmid and either empty vector, Rta expression plasmid, Zta expression plasmid, or a mixture of both Zta and Rta plasmids, and luciferase activity was measured in cell lysates 24 h after transfection. RQ was calculated as the ratio of signal in transactivator-transfected cells to empty vector-transfected cells. (C) The effect of either Zta, Rta, or both genes on ACE2 promoter activity was assessed in 293T cells by cotransfection and luciferase assay as for panel B. Expression of each transactivator was confirmed by immunoblotting with anti-Zta or anti-Rta antibodies, as shown on the right, with tubulin as a loading control. *P* values for each comparison are shown by letters above each bar. Nonsignificant differences ($P > 0.5$) are denoted with the same letter. Significant differences ($P < 0.0001$) are denoted by different letters.

EBV Zta induces endogenous ACE2 expression in EBV-negative cells. To further confirm that Zta is the key inducer of endogenous ACE2 expression, we generated an EBV-uninfected AGS cell line that stably expresses doxycycline-inducible Zta. These cells robustly produce Zta within 24 h when treated with doxycycline. When Zta was induced, it significantly upregulated ACE2 mRNA expression compared to mock-induced cells (Fig. 4D), which demonstrates that Zta alone can induce cellular ACE2.

The EBV transcriptional activator Zta acts on the ACE2 promoter through a noncanonical response element. The three potential ZREs identified in the ACE2 promoter are not predicted to contain CpG methylation sites and were therefore deemed unlikely to mediate the methylation-dependent Zta responsiveness that was observed. Zta response elements that do not contain canonical ZRE sequences have been identified in cellular promoters (32). We therefore mapped the Zta-responsive region of the ACE2 promoter by site-directed mutagenesis and deletion of regions of the promoter.

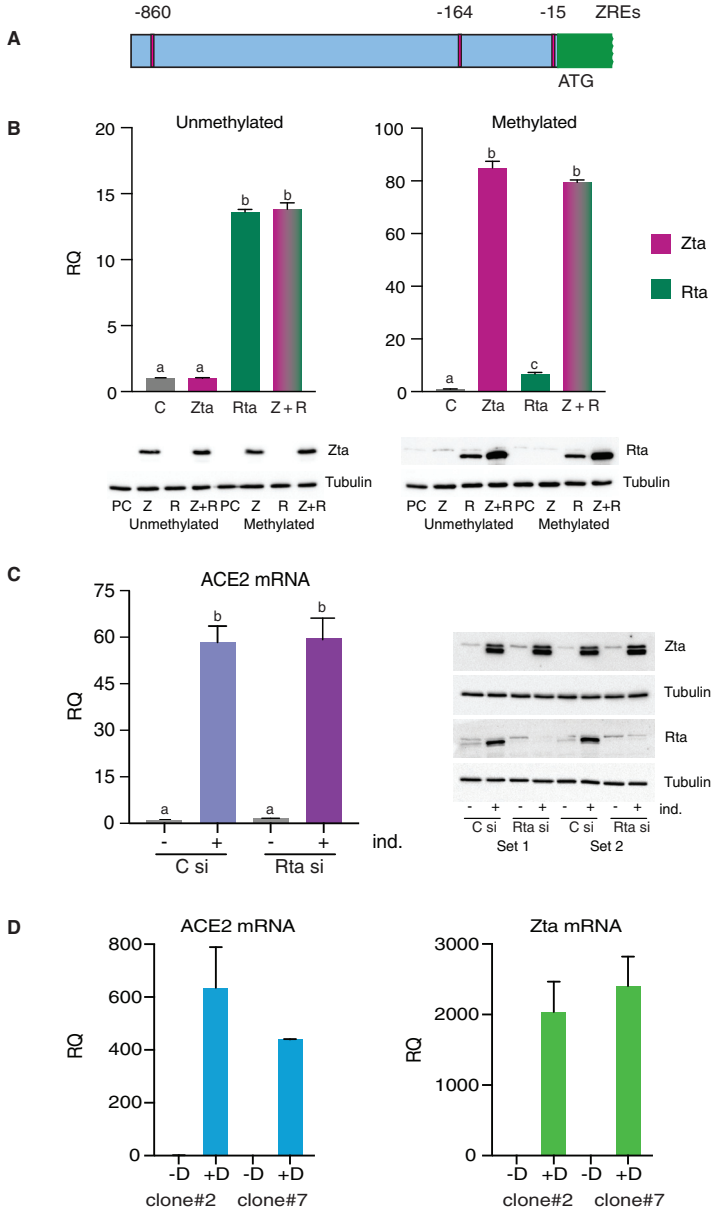

FIG 4 Methylation of the ACE2 promoter affects activation by Zta and Rta. (A) The ACE2 promoter contains 3 Zta response elements. Consensus EBV Zta binding sites known to mediate Zta responsiveness are shown in the region upstream of the ACE2 coding region. (B) The ACE2 promoter plasmid was either methylated *in vitro* with CpG methyltransferase M.SssI or not methylated prior to cotransfection with either empty vector, the Zta or Rta transactivator, or both Zta and Rta, as shown. Luciferase assays were performed 24 h after transfection, and RQ was calculated as in Fig. 3. For all experiments, data are the means and standard errors of the means for three independent experiments, with luciferase assays performed in technical triplicates for each sample. Western blots confirming equal expression of Zta and Rta are shown below each panel with tubulin as a loading control. RQ, relative quantity. (C) Effect of Rta depletion on ACE2 expression after EBV induction was measured by RT-PCR of RNA harvested from siRNA-transfected cells. Cells were transfected with either nontargeting control siRNA (Csi) or Rta-specific siRNA (Rta si) prior to induction of EBV replication (ind.). All experiments were performed in triplicate transfections, and all assays were performed in technical triplicates for each sample. Lysates were immunoblotted with anti-Rta antibody to confirm depletion of Rta protein in Rta siRNA-transfected cells and with anti-Zta antibody to confirm equal expression of Zta. Tubulin is shown below each blot as a loading control. *P* values for each comparison are shown by letters above each bar. Nonsignificant differences ($P > 0.1$) are denoted with the same letter. Significant differences ($P \leq 0.001$) are denoted by different letters except that in panel B, the *P* value for the difference between control and Rta with a methylated target was 0.0004. (D) Effect of EBV Zta on endogenous ACE2 expression in EBV-negative cells. Two independently derived clones (no. 2 and 7) of Zta-inducible, EBV-negative AGSiZ cells were treated with doxycycline or mock treated to induce Zta

(Continued on next page)

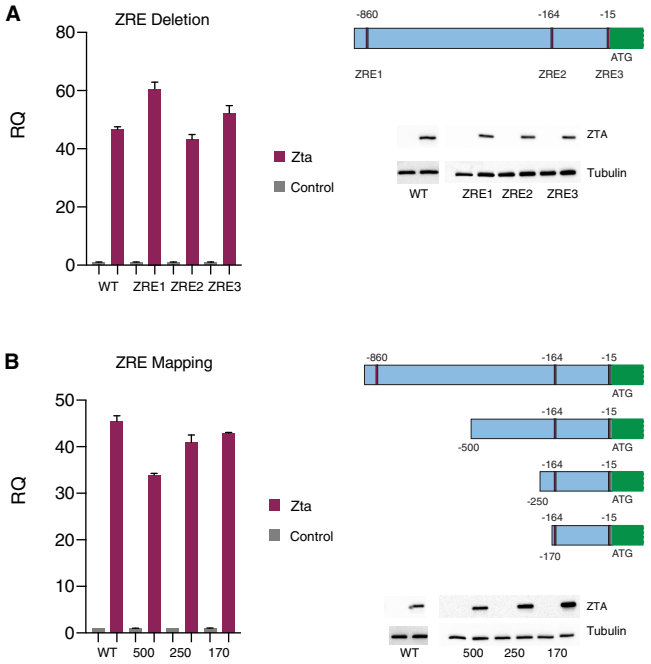

FIG 5 Mapping of the Zta response element in the ACE2 promoter. (A) The three canonical ZREs in the ACE2 promoter (shown in maroon on the right) were individually deleted from the ACE2 promoter. The resulting mutant promoter-reporter plasmids or parent wild-type ACE2 plasmids were methylated *in vitro* and transfected into 293 cells with either Zta or empty vector, and promoter activity was measured by luciferase assay. Expression of Zta was confirmed by immunoblotting with tubulin as a loading control. RQ, relative quantity. (B) Sequential truncations of the ACE2 promoter were made as shown, and each was cloned into the luciferase reporter plasmid. The truncated promoter constructs were methylated *in vitro*, transfections with either Zta plasmid or empty vector were performed, and promoter activity was measured as for panel A. Immunoblots for Zta and tubulin are shown on the right.

Each of the three potential ZREs was also individually deleted from the ACE2 promoter in the luciferase reporter plasmid, methylated *in vitro*, and cotransfected with Zta in 293 cells. As shown in Fig. 5A, deletion of each ZRE sequence did not affect transactivation of the reporter by Zta.

We next mapped the minimal promoter that was Zta responsive by sequential deletion of the ACE2 promoter. As shown in Fig. 5B, Zta responsiveness mapped to a 170-nucleotide (nt) region upstream of the coding region. Since this region does not contain methylated ZREs, and the ZREs that are present are not required for Zta responsiveness, these data indicate that Zta activates the ACE2 promoter either indirectly or through a noncanonical response element(s).

Infection of NOK cells with EBV enhances SARS-CoV-2 pseudovirus entry. *In vivo*, EBV released from circulating B lymphocytes is thought to infect epithelial cells in the nasopharynx and oral epithelium, resulting in lytic EBV replication and lytic gene expression. To recapitulate this sequence of events, we infected EBV-negative normal oral keratinocytes immortalized with h-TERT (NOK cells) with EBV *in vitro* and examined the effect on Zta expression, ACE2 expression, and SARS-CoV-2 pseudovirus entry. NOK cells grown in 6-well plates were mock infected or infected with green fluorescent protein (GFP)-expressing Akata EBV by spinoculation as previously described (10). Cells were visually examined and photographed under fluorescence microscopy to detect

FIG 4 Legend (Continued)
expression in triplicate experiments. The cells were harvested 48 h after induction, and RNA was isolated. ACE2 and Zta mRNA expression was measured by RT-PCR in technical triplicates for each sample. RQ, relative quantity of each specific mRNA compared to uninduced cell levels. *P* values for the difference between uninduced and induced values were ≤0.002 for both Zta and ACE2.

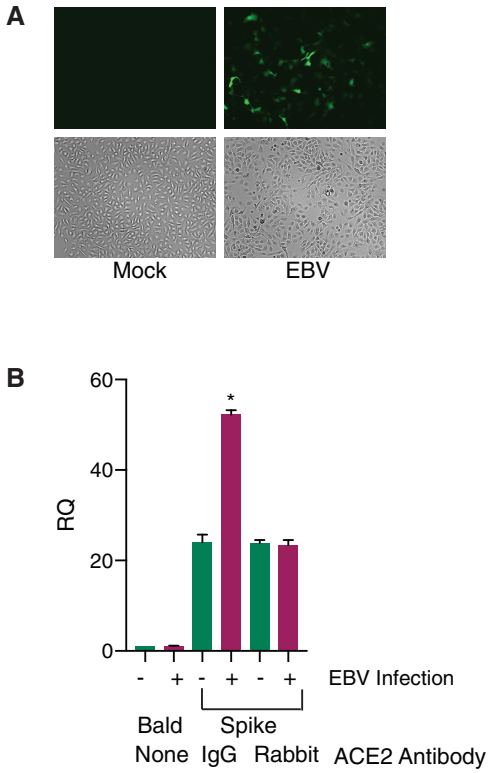

FIG 6 Infection of NOK cells with EBV leads to induction of ACE2. (A) Infection of NOK cells with recombinant GFP-Akata EBV leads to infection and GFP expression in NOK cells. NOK cells plated on slides were infected with Akata virus or mock infected and examined by fluorescence and phase-contrast microscopy 3 days after infection. (B) Cells infected with Akata EBV or mock infected were infected with SARS-CoV-2 PV 72 h after EBV infection. For antibody blockade, cells were treated with either anti-ACE2 antibody or control IgG 2 h prior to infection with PV. Cells were harvested 24 h after PV infection, and PV entry was measured by luciferase assay. RQ, relative quantity.

GFP expression in EBV-infected cells at 3 days postinfection. Approximately 10% of NOK cells exhibited GFP expression, indicating infection by EBV (Fig. 6A). To determine whether lytic EBV replication in a minority of the infected NOK cells led to an overall increase SARS-CoV-2 PV infection, we compared the entry of SARS-CoV-2 PV in EBV-infected and mock-infected NOK cell cultures. As shown in Fig. 6B, EBV infection led to a >2-fold increase in SARS-CoV-2 PV entry that was blocked by ACE2 antibody.

DISCUSSION

We have shown that EBV lytic replication in epithelial cells induces transcription of ACE2 via the EBV transactivator protein Zta. The Zta responsiveness of the ACE2 promoter suggests that the ability of EBV to regulate ACE2 may benefit the virus by enhancing efficiency of EBV production, possibly through the antiapoptotic functions of ACE2 (33–35). Unlike most transcriptional activators, Zta is preferentially active when its target promoters are methylated (27, 29, 36). During latency, the EBV genome exists as a nuclear episome which is highly chromatinized and methylated (30, 37). The unusual preferential activity of Zta on methylated promoters is thought to allow Zta activation of such epigenetically silenced EBV lytic promoters present in the viral genome during latency. Zta's ability to preferentially activate the methylated ACE2 promoter suggests that this property may also be important in activating ACE2 expression and possibly expression of other epigenetically silenced cellular genes when EBV infects epithelial cells and enters the lytic cycle.

Infection of epithelial cells by SARS-CoV-2 is highly dependent on surface ACE2 expression (1–3). SARS-CoV-2 infectivity is highest in nasal epithelium, in which greater

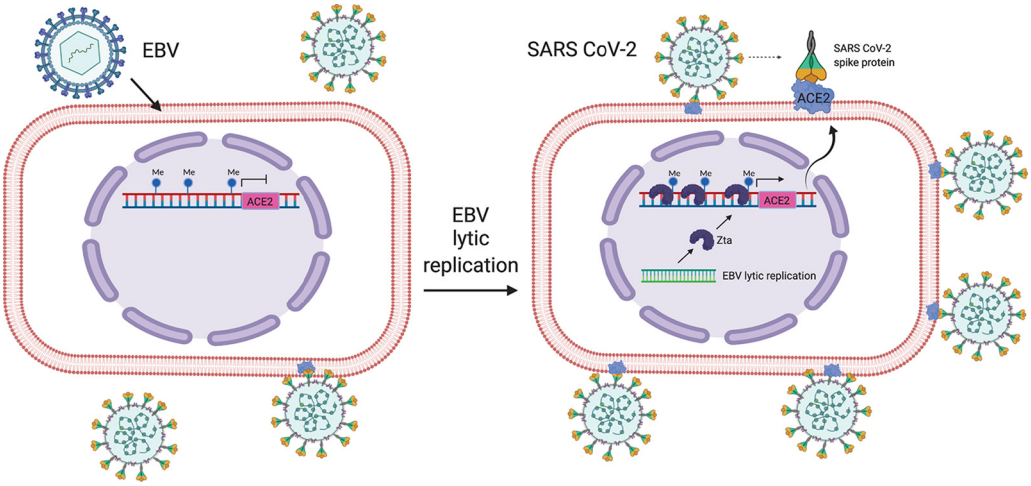

FIG 7 Model for effect of EBV replication on SARS-CoV-2 infection. EBV infecting an epithelial cell is shown at left with a methylated and epigenetically silenced ACE2 promoter. Limited ACE2 expression and SARS-CoV-2 binding are shown. Upon EBV lytic replication, the EBV Zta transactivator is expressed, binds, and activates the methylated ACE2 promoter, leading to increased ACE2 expression and SARS-CoV-2 binding.

ACE2 expression has been detected than in airway epithelium (4, 5). The factors that govern ACE2 expression in humans remain to be fully characterized, but variability in ACE2 expression appears to be age dependent and subject to epigenetic regulation by methylation (31, 38). Susceptibility to SARS-CoV-2 infection is also highly variable, and the factors that govern differences among individuals are not well understood. We propose that EBV may play a role in variability of ACE2 expression in oropharyngeal and nasopharyngeal epithelium by reactivating epigenetically silenced ACE2 genes. This model by which EBV infection and entry into lytic replication may induce ACE2 expression and enhance SARS-CoV-2 susceptibility in human oral epithelium is shown in Fig. 7. While EBV replication may enhance SARS-CoV-2 entry, its potential effects on subsequent steps in coronavirus replication remain unknown and require further investigation.

EBV persistently and subclinically infects the majority of the human population (7). While the site of EBV latency is the memory B lymphocyte, EBV shuttles between B cells and epithelial cells of the oropharynx (6), where it undergoes lytic replication, and spreads to other epithelial cells (39, 40). Such cycles of lytic replication occur stochastically and result in various amounts of lytic gene expression and viral shedding in normal hosts at any given time. There is a significant variability in such permissiveness for lytic replication, ranging from 23 to 72% in individuals (41). However, quantitative and sensitive sequential measurements of viral shedding indicate that all EBV-positive individuals continuously undergo oral epithelial cell EBV lytic replication and release of virus, although EBV shedding may vary by up to 5 orders of magnitude from one time point to another (39). Our findings that EBV reactivation and EBV lytic replication enhance ACE2 expression and thereby increase SARS-CoV-2 infection efficiency raise the possibility that epithelial cell replication of EBV, which occurs spontaneously, intermittently, and asymptomatically in >90% of adults (7), may affect susceptibility to SARS-CoV-2. These findings suggest that pharmacologically inhibiting EBV reactivation *in vivo* could reduce transmission and severity of SARS-CoV-2 in the human population.

MATERIALS AND METHODS

Cell lines and plasmids. Cells of the gastric carcinoma cell line AGS were infected with GFP-expressing EBV Akata BX1 virus to generate the stably EBV-infected cell line AGS-BX1 (11). AGSiZ was derived from AGS-BX1 by stably transducing it with a lentivirus expressing the doxycycline-inducible EBV lytic transactivator protein Zta, which induces lytic replication and infectious-virion production (10). AGSiZ cells were cultured in Ham's F-12 medium with 10% (vol/vol) fetal bovine serum (FBS) (tetracycline system-approved FBS; Clontech no. 631106), 1% GlutaMAX (Life Technologies), 0.5 mg/ml neomycin, and

0.5 μg/ml puromycin. HEK293T cells were grown in Dulbecco's modified Eagle medium (DMEM) supplemented with 10% (vol/vol) FBS. EBV lytic replication in AGSiZ cells was induced by addition of 1.0 μg/ml doxycycline (Sigma; D9891). NOK cells (gift from S. Kenney) were generated by h-TERT immortalization of normal human oral keratinocytes and were maintained in an undifferentiated state by culturing them in keratinocyte serum-free medium (KSFM) supplemented with human epidermal growth factor and bovine pituitary extract (Life Technologies) (42). An EBV-negative AGSiZ cell line stably expressing doxycycline-inducible BZLF1 (Zta) was constructed by lentiviral transduction as reported previously (10). For lentivirus production, 293T cells were transfected with lentiviral vector containing the B95.8 EBV BZLF1 coding sequence along with packaging plasmids as reported previously (43). A total of 250,000 AGS cells were plated in 6-well plates in F-12 medium supplemented with tetracycline system-approved FBS (Clontech no. 631106) and 1% GlutaMAX from Life Technologies (no. 35050-061). The next day, cells were infected with 500 μl of lentiviral supernatant by spin inoculation as reported previously (10, 43). The next day, cells were split, and transduced cells were selected with medium containing 1.0 μg/ml puromycin. The medium was changed every 3 days with fresh selection for 2 weeks. The individual clones were grown and tested for Zta expression by Western blotting at 48 h after addition of doxycycline.

To generate an Rta expression vector, 1.818 kb of B95-8 EBV cDNA (nt 91078 to 92895; accession no. NC_007605.1) was amplified by high-fidelity PCR and cloned into pCDNA3 (Invitrogen) at the EcoRV site (44). The Zta gene was PCR amplified from Akata EBV DNA isolated from AGSiZ. A 974-bp fragment was amplified (nt 89581 to 90554; accession no. KC207813.1) and cloned into the EcoRV site of pCDNA3. All cell lines were tested for *Mycoplasma* contamination with a Lonza MycoAlert mycoplasma detection kit (catalog no. LT07-418).

RNA isolation and qPCR. AGSiZ cells were plated in six-well plates, and EBV lytic replication was induced by addition of 1 μg/ml doxycycline. Cells were harvested at different times after lytic induction as indicated for individual experiments. Total RNA was isolated from washed cell pellets, lysed in 700 μl of Qiazol, and purified with miRNeasy columns according to the manufacturer's protocols. Quantitative reverse transcription-PCR (qPCR) was performed with the Power SYBR green RNA-to-CT 1-Step kit (Applied Biosystems). qPCR was performed in triplicate from each biological sample, and the relative quantity (RQ) for each gene was calculated using cellular GAPDH (glyceraldehyde-3-phosphate dehydrogenase) as an endogenous control in all reactions.

Data for qPCR were analyzed using GraphPad Prism 8 software. The error bars in the figures indicate the standard errors of the means (SEM) from three different biological replicates. *P* values were calculated using unpaired *t* tests. The gene-specific primers were as follows: ACE2-Q1F, 5′-TGGGACTCTGCCATTTACTTAC-3′; ACE2-Q1R, 5′-CCCAACTATCTCTCGCTTCATC-3′; BMRF1 Q1F, 5′-ATACGGTCAGTCCATCTCCT-3′; BMRF1 Q1R, 5′-CACTTTCTTGGGGTGCTT-3′; BcLF1 Q1F, 5′-GTGGATCAGGCCGTTATTGA-3′; BcLF1 Q1R, 5′-CCTCAAACCCGT GGATCATA-3′.

RNA isolation, sequencing, and bioinformatic analysis. cDNA libraries were prepared from poly(A) RNA and were sequenced on a HiSeq 2500 instrument with 50-cycle single-end reads. Sequenced reads obtained from EBV-infected AGS cells (AGSiZ) were aligned to the EBV Akata 1 (GenBank accession no. KC207813.1) genome. Raw counts were estimated using USeq's Defined Region Differential Seq application. The raw counts were reanalyzed using DESeq2 version 1.26.0 to identify differentially expressed genes at 24 and 48 h with a 5% false discovery rate. Enriched pathways were identified using gene set enrichment analysis and Ingenuity Pathway Analysis.

Depletion of EBV Rta by siRNA transfection. EBV Rta knockdown (KD) was performed with siRNAs designed using the RNA interference (RNAi) design tool Custom Dicer-Substrate siRNA (DsiRNA) (IDT) and synthesized by IDT. Sequences of the siRNA used for EBV Rta KD were as follows: sense strand, 5′ AAA UCU UGG AUA CAU UUC UAA ATG A 3′; antisense strand, 5′ UCA UUU AGA AAU GUA UCC AAG AUU UCA 3′.

The last two nucleotides of the sense strand were DNA. KD in AGSiZ cells was performed by transfecting specific siRNAs targeting Rta or with negative-control siRNA (51-01-14-04; IDT) with Lipofectamine RNAiMAX transfection reagent (Invitrogen; no. 13778150) according to the manufacturer's protocols. Lytic EBV reactivation was induced in AGSiZ cells with doxycycline 3 h after siRNA transfection.

Immunoblotting for EBV Zta and Rta. A total of 250,000 AGSiZ cells were plated on six-well plates 1 day before induction. Cells were treated with doxycycline to induce EBV lytic induction. 293 or EBV-negative AGS cells were transfected with plasmids as indicated in each experiment. Whole-cell lysates were prepared 48 h after EBV lytic induction or transfection and analyzed by Western blotting with anti-Zta (Santa Cruz; sc53904), anti-Rta (Argene; 11-008), or antitubulin (Sigma; SAB3501072) antibodies. The signal was visualized by incubation with horseradish peroxidase-conjugated anti-mouse or anti-rabbit secondary antibody using Bio-Rad chemiluminescence detection reagent.

Human ACE2 reporter construction and luciferase assays. Nine hundred ninety-four base pairs of the ACE2 promoter sequence (bp −894 to +100 relative to the ACE2 start codon) was PCR amplified from genomic DNA isolated from AGSiZ cells using a blood and tissue DNeasy kit (Qiagen). Restriction enzyme sites for BglII and NcoI were added to the PCR amplicon on the 5′ and 3′ ends, respectively, by incorporating the restriction endonuclease restriction site sequences in the PCR primers. The ACE2 promoter was ligated into the BglII and NcoI sites in pGL3 Basic (Promega) between like enzyme sites. The first 100 nucleotides of the ACE2 coding domain were cloned in frame with the coding domain of luciferase in pGL3. Plasmids were purified using the Qiagen Hi Speed Midiprep kit and sequenced. The primers used for the amplification of the ACE2 promoter were as follows: pACE2 F, 5′ TTA GAT CTA AAT TAA AAC TGA TCA GAA ATG GCT GGG 3′; pACE2 R 5′ AAC CAT GGG GTT AAA CTT GTC CAA AAA TG 3′.

For mapping of the Zta response element in the ACE2 promoter, truncations of the promoter fragment and mutations of each individual canonical ZRE were generated the pACE2-pGL3 Basic plasmid

using a Q5 site-directed mutagenesis kit (NEB) according to the manufacturer's protocol. The following primers were used for removal of each of the ZRE sites: 1-Q5 ZRE1 F, CGC CTG TAA TCC TAG CAC; Q5 ZRE1 R, CTG TGC CCA GCC ATT TCT; 2-Q5 ZRE2 F, GCA GAT TGT TTA CTG TGT TC; Q5 ZRE2 R, ATA TAA AGT TCA TCC TGG AG; 3-Q5 ZRE3 F, CAG GGG ACG ATG TCA AGC; Q5 ZRE3 R, AGA TCA CAT CCA CTG AAT GAC. Truncations were done with the following primers: Q5 pACE2 R, AGA TCT CGA GCC CGG GCT (universal for all); Q5 pACE2 -500 F, GTA GAG AGT TTC TGG GAA TAT GAT CTT GAA ATA AAA ATA AAT G, Q5 pACE2 −250 F, AAT AAC GTA TTC TTA TTT GAT TCA CTT TAA AAA ATT ATT CTA AAA TCT GTT AC; Q5 pACE2 −170 F, TAT ATT GGC TCA GCA GAT TGT TTA CTG TG.

ACE2 promoter plasmid was transfected into one of 3 cell lines, AGSiZ, EBV-negative AGS, or 293T. AGSiZ cells were transfected with the reporter plasmid 24 h after induction with 1.0 μg/ml doxycycline. AGS cells and 293T cells were cotransfected with empty vector, EBV Zta-expressing vector, EBV Rta-expressing vector, or both Zta and Rta vectors. All transfections were done in triplicate using Transit 293 reagent (Mirus) and 1 μg of plasmid DNA per the manufacturer's protocol. At 48 h after transfection, samples were harvested and lysed in 1× reporter lysis buffer (Promega) using the manufacturer's protocol. Five microliters of cleared supernatant was added to 15 μl of firefly luciferase reagent and read using a luminometer (Turner Biosystems; 20/20n). Each transfection was performed in triplicate, and three technical replicates were assayed for each biological replicate. The readings were used to calculate a relative quotient (RQ) relative to either empty vector-transfected sample or uninduced sample, respectively.

In vitro methylation of plasmids was performed by incubating 10 μg of ACE2 promoter plasmid with CpG methyltransferase (M.SssI) (New England Biolabs [NEB]) with *S*-adenosylmethionine for 30 min at 37°C. An unmethylated control plasmid was processed in tandem. After methylation, heat inactivation of the methylase was performed and plasmid DNA was ethanol precipitated and quantitated by spectrophotometry. Transfections with methylated DNA were performed in 293T cells as described above using Transit 293 reagent with cotransfection of Zta, Rta, or both expression vectors. Luciferase assays were performed in technical triplicates with lysates harvested 12 h after transfection.

Fluorescence microscopy. A total of 200,000 NOK cells were plated in 6-well plates and were either mock infected or infected with EBV Akata virus at a multiplicity of infection (MOI) of 5 per cell by spin inoculation as described previously (10). Cells were visually examined and photographed under fluorescence microscopy to detect GFP expression in EBV-infected cells at 3 days postinfection.

SARS-CoV-2 spike, Junin G, and bald pseudovirus production, purification, infection, and blocking with ACE2 antibodies. 293T cells were plated in 100-mm plates at a density to reach 80% confluence the following day. The plates were transfected with either 6 μg of SARS-CoV-2-spike plasmid, JunV-GP plasmid (16) (both gifts from Tom Gallagher, Loyola University), or pCDNA3 vector plasmid (Invitrogen) using Transit 293 (Mirus). Cells were incubated for 6 h; medium was replaced with fresh DMEM–10% fetal calf serum (FCS) (DMEM-10), and cells were grown overnight. The following day, each plate was infected with 60 μl of transducing particle (VSVΔG-Fluc pseudotyped with Junin virus [JUNV] G protein) in 6 ml of fresh prewarmed DMEM-10. Infected cells were incubated for 2 h and then rinsed three times with warm serum-free DMEM. Six milliliters of prewarmed DMEM-10 was added, and cells were incubated overnight. Each day for the next 3 days, supernatant was collected in 15-ml centrifuge tubes, and 6 ml of fresh DMEM-10 was added. Each supernatant was spun at 300 × *g* for 10 min, transferred to a fresh tube, and spun at 3,000 × *g* for 10 min. Supernatants from each daily harvest were stored at −80°C until being pooled for concentration. Supernatants containing pseudovirus were thawed and pooled in an ultracentrifuge tube. Using a 3-ml syringe, a cushion of 1.5 ml 20% sucrose was added to the bottom of the tube. Tubes were centrifuged at 5,600 × *g* for 18 h at 4°C. The supernatant was carefully removed, and 180 μl of serum-free medium was used to gently resuspend the pellet by leaving the tube in a cooled centrifuge rotor for 2 h followed by gentle pipetting. After proper resuspension, 100× concentrated and purified pseudovirus was divided into 60-μl aliquots in cryovials and frozen at −80°C until use.

Pseudovirus infections were performed in 96-well plates by plating AGSiZ, NOK, or 293T cells in 100 μl of medium appropriate for each cell line. For experiments to measure the effect of ACE2 expression on pseudovirus infection, infections were performed 24 h after either induction of EBV replication or ACE2 transfection. AGSiZ cells were induced by adding 100 μl of 2.0 μg/ml doxycycline (for a final concentration of 1.0 μg/ml). 293T cells were transfected with either empty vector or ACE2 expression vector. At 48 h after induction or transfection, medium was removed and pseudovirus infections were carried out. To measure the effect of EBV infection on ACE2-mediated pseudovirus entry into NOK cells, NOK cells were either infected or mock infected with Akata virus produced from AGSiZ at a final MOI of 5 (~50,000 pseudovirions per 10,000 cells/well). For antibody treatments prior to pseudovirus infection, antibody was added to a final concentration of 20 μg/ml. ACE2 antibodies used were goat (R&D Systems; AF933) or rabbit (Thermo Fisher; PA5-20040). Rabbit IgG (Bethyl; P120-101) was used as a control at the same concentration. After treatment with antibody for 2 h, 0.6 μl of concentrated pseudovirus preparation was added to each well. A no-virus control was done in parallel. After 4 h of incubation with pseudovirus particles to allow pseudovirus entry, the medium was removed and replaced with 100 μl of complete medium, and cells were incubated overnight. Supernatants were then removed, and 50 μl of cell lysis reagent (Promega) was added to the wells. After incubation at room temperature for 15 min, plates were sealed with Parafilm and frozen at −80°C. Cell lysates were thawed, transferred to a fresh 1.5-ml centrifuge tube, and spun at 700 × *g* for 5 min. Five microliters of cleared supernatant was added to 15 μl of firefly luciferase reagent (Promega) and read using a luminometer (Turner Biosystems; 20/20n); three technical triplicates were performed for each sample. Each biological triplicate was used to determine an RQ relative to the bald virus control for each sample.

Data availability. All sequencing data that support the findings of this study have been deposited in the National Center for Biotechnology Information Gene Expression Omnibus (GEO) and are accessible through the GEO Series accession number GSE155811.

ACKNOWLEDGMENTS

This work was supported by NCI R01 81133 to S.S. and a Department of Internal Medicine Academic Seed Grant, University of Utah (D.V.).

We thank Chris Stubben for bioinformatic analysis of RNA sequencing data and Zola Wagner for expert technical assistance. The Huntsman Cancer Institute High-Throughput Genomics and Bioinformatic Analysis was used for all high-throughput RNA and DNA sequencing and analysis.

REFERENCES

1. Letko M, Marzi A, Munster V. 2020. Functional assessment of cell entry and receptor usage for SARS-CoV-2 and other lineage B betacoronaviruses. Nat Microbiol 5:562–569. https://doi.org/10.1038/s41564-020-0688-y.
2. Li W, Moore MJ, Vasilieva N, Sui J, Wong SK, Berne MA, Somasundaran M, Sullivan JL, Luzuriaga K, Greenough TC, Choe H, Farzan M. 2003. Angiotensin-converting enzyme 2 is a functional receptor for the SARS coronavirus. Nature 426:450–454. https://doi.org/10.1038/nature02145.
3. Zhou P, Yang X-L, Wang X-G, Hu B, Zhang L, Zhang W, Si H-R, Zhu Y, Li B, Huang C-L, Chen H-D, Chen J, Luo Y, Guo H, Jiang R-D, Liu M-Q, Chen Y, Shen X-R, Wang X, Zheng X-S, Zhao K, Chen Q-J, Deng F, Liu L-L, Yan B, Zhan F-X, Wang Y-Y, Xiao G-F, Shi Z-L. 2020. A pneumonia outbreak associated with a new coronavirus of probable bat origin. Nature 579:270–273. https://doi.org/10.1038/s41586-020-2012-7.
4. Xu H, Zhong L, Deng J, Peng J, Dan H, Zeng X, Li T, Chen Q. 2020. High expression of ACE2 receptor of 2019-nCoV on the epithelial cells of oral mucosa. Int J Oral Sci 12:8. https://doi.org/10.1038/s41368-020-0074-x.
5. Hou YJ, Okuda K, Edwards CE, Martinez DR, Asakura T, Dinnon KH, 3rd, Kato T, Lee RE, Yount BL, Mascenik TM, Chen G, Olivier KN, Ghio A, Tse LV, Leist SR, Gralinski LE, Schäfer A, Dang H, Gilmore R, Nakano S, Sun L, Fulcher ML, Livraghi-Butrico A, Nicely NI, Cameron M, Cameron C, Kelvin DJ, de Silva A, Margolis DM, Markmann A, Bartelt L, Zumwalt R, Martinez FJ, Salvatore SP, Borczuk A, Tata PR, Sontake V, Kimple A, Jaspers I, O'Neal WK, Randell SH, Boucher RC, Baric RS. 2020. SARS-CoV-2 reverse genetics reveals a variable infection gradient in the respiratory tract. Cell 182:429–446.e414. https://doi.org/10.1016/j.cell.2020.05.042.
6. Borza CM, Hutt-Fletcher LM. 2002. Alternate replication in B cells and epithelial cells switches tropism of Epstein-Barr virus. Nat Med 8:594–599. https://doi.org/10.1038/nm0602-594.
7. Longnecker RM, Kieff E, Cohen JI. 2013. Epstein-Barr virus, p 1898–1959. In Knipe DM, Howley PM (ed), Fields virology, 5th ed, vol 2. Wolters Kluwer/Lippincott Williams and Wilkins, Philadelphia, PA.
8. Kenney S, 2007. Reactivation and lytic replication of EBV, p 403–433. In Arvin A, Campardelli-Fiume G, Mocarski E, Moore PS, Roizman B, Whitley R, Yamanishi K (ed), Human herpesviruses: biology, therapy, and immunoprophylaxis, vol 25. Cambridge University Press, Cambridge, MA.
9. Li D, Fu W, Swaminathan S. 2018. Continuous DNA replication is required for late gene transcription and maintenance of replication compartments in gammaherpesviruses. PLoS Pathog 14:e1007070. https://doi.org/10.1371/journal.ppat.1007070.
10. Verma D, Thompson J, Swaminathan S. 2016. Spironolactone blocks Epstein-Barr virus production by inhibiting EBV SM protein function. Proc Natl Acad Sci U S A 113:3609–3614. https://doi.org/10.1073/pnas.1523686113.
11. Molesworth SJ, Lake CM, Borza CM, Turk SM, Hutt-Fletcher LM. 2000. Epstein-Barr virus gH is essential for penetration of B cells but also plays a role in attachment of virus to epithelial cells. J Virol 74:6324–6332. https://doi.org/10.1128/JVI.74.14.6324-6332.2000.
12. Chevallier-Greco A, Manet E, Chavrier P, Mosnier C, Daillie J, Sergeant A. 1986. Both Epstein-Barr virus (EBV)-encoded trans-acting factors, EB1 and EB2, are required to activate transcription from an EBV early promoter. EMBO J 5:3243–3249. https://doi.org/10.1002/j.1460-2075.1986.tb04635.x.
13. Countryman J, Miller G. 1985. Activation of expression of latent Epstein-Barr herpesvirus after gene transfer with a small cloned subfragment of heterogeneous viral DNA. Proc Natl Acad Sci U S A 82:4085–4089. https://doi.org/10.1073/pnas.82.12.4085.
14. Takada K, Shimizu N, Sakuma S, Ono Y. 1986. trans activation of the latent Epstein-Barr virus (EBV) genome after transfection of the EBV DNA fragment. J Virol 57:1016–1022. https://doi.org/10.1128/JVI.57.3.1016-1022.1986.
15. Summers WC, Klein G. 1976. Inhibition of Epstein-Barr virus DNA synthesis and late gene expression by phosphonoacetic acid. J Virol 18:151–155. https://doi.org/10.1128/JVI.18.1.151-155.1976.
16. Park JE, Li K, Barlan A, Fehr AR, Perlman S, McCray PB, Jr, Gallagher T. 2016. Proteolytic processing of Middle East respiratory syndrome coronavirus spikes expands virus tropism. Proc Natl Acad Sci U S A 113:12262–12267. https://doi.org/10.1073/pnas.1608147113.
17. Shang J, Ye G, Shi K, Wan Y, Luo C, Aihara H, Geng Q, Auerbach A, Li F. 2020. Structural basis of receptor recognition by SARS-CoV-2. Nature 581:221–224. https://doi.org/10.1038/s41586-020-2179-y.
18. Zalani S, Holley-Guthrie E, Kenney S. 1996. Epstein-Barr viral latency is disrupted by the immediate-early BRLF1 protein through a cell-specific mechanism. Proc Natl Acad Sci U S A 93:9194–9199. https://doi.org/10.1073/pnas.93.17.9194.
19. Feederle R, Kost M, Baumann M, Janz A, Drouet E, Hammerschmidt W, Delecluse HJ. 2000. The Epstein-Barr virus lytic program is controlled by the co-operative functions of two transactivators. EMBO J 19:3080–3089. https://doi.org/10.1093/emboj/19.12.3080.
20. Kenney SC, Mertz JE. 2014. Regulation of the latent-lytic switch in Epstein-Barr virus. Semin Cancer Biol 26:60–68. https://doi.org/10.1016/j.semcancer.2014.01.002.
21. Adamson AL, Darr D, Holley-Guthrie E, Johnson RA, Mauser A, Swenson J, Kenney S. 2000. Epstein-Barr virus immediate-early proteins BZLF1 and BRLF1 activate the ATF2 transcription factor by increasing the levels of phosphorylated p38 and c-Jun N-terminal kinases. J Virol 74:1224–1233. https://doi.org/10.1128/jvi.74.3.1224-1233.2000.
22. Gruffat H, Sergeant A. 1994. Characterization of the DNA-binding site repertoire for the Epstein-Barr virus transcription factor R. Nucleic Acids Res 22:1172–1178. https://doi.org/10.1093/nar/22.7.1172.
23. Quinlivan EB, Holley-Guthrie EA, Norris M, Gutsch D, Bachenheimer SL, Kenney SC. 1993. Direct BRLF1 binding is required for cooperative BZLF1/BRLF1 activation of the Epstein-Barr virus early promoter, BMRF1. Nucleic Acids Res 21:1999–2007. https://doi.org/10.1093/nar/21.8.1999.
24. Gutsch DE, Marcu KB, Kenney SC. 1994. The Epstein-Barr virus BRLF1 gene product transactivates the murine and human c-myc promoters. Cell Mol Biol (Noisy-le-grand) 40:747–760.
25. Li Y, Webster-Cyriaque J, Tomlinson CC, Yohe M, Kenney S. 2004. Fatty acid synthase expression is induced by the Epstein-Barr virus immediate-early protein BRLF1 and is required for lytic viral gene expression. J Virol 78:4197–4206. https://doi.org/10.1128/JVI.78.8.4197-4206.2004.
26. Adamson AL, Kenney SC. 1998. Rescue of the Epstein-Barr virus BZLF1 mutant, Z(S186A), early gene activation defect by the BRLF1 gene product. Virology 251:187–197. https://doi.org/10.1006/viro.1998.9396.
27. Bhende PM, Seaman WT, Delecluse HJ, Kenney SC. 2004. The EBV lytic switch protein, Z, preferentially binds to and activates the methylated viral genome. Nat Genet 36:1099–1104. https://doi.org/10.1038/ng1424.
28. Wille CK, Nawandar DM, Panfil AR, Ko MM, Hagemeier SR, Kenney SC. 2013. Viral genome methylation differentially affects the ability of BZLF1 versus BRLF1 to activate Epstein-Barr virus lytic gene expression and viral replication. J Virol 87:935–950. https://doi.org/10.1128/JVI.01790-12.
29. Bergbauer M, Kalla M, Schmeinck A, Göbel C, Rothbauer U, Eck S, Benet-Pagès A, Strom TM, Hammerschmidt W. 2010. CpG-methylation regulates

a class of Epstein-Barr virus promoters. PLoS Pathog 6:e1001114. https://doi.org/10.1371/journal.ppat.1001114.
30. Kalla M, Schmeinck A, Bergbauer M, Pich D, Hammerschmidt W. 2010. AP-1 homolog BZLF1 of Epstein-Barr virus has two essential functions dependent on the epigenetic state of the viral genome. Proc Natl Acad Sci U S A 107:850–855. https://doi.org/10.1073/pnas.0911948107.
31. Fan R, Mao SQ, Gu TL, Zhong FD, Gong ML, Hao LM, Yin FY, Dong CZ, Zhang LN. 2017. Preliminary analysis of the association between methylation of the ACE2 promoter and essential hypertension. Mol Med Rep 15:3905–3911. https://doi.org/10.3892/mmr.2017.6460.
32. Chang Y, Lee HH, Chen YT, Lu J, Wu SY, Chen CW, Takada K, Tsai CH. 2006. Induction of the early growth response 1 gene by Epstein-Barr virus lytic transactivator Zta. J Virol 80:7748–7755. https://doi.org/10.1128/JVI.02608-05.
33. Bao H, Gao F, Xie G, Liu Z. 2015. Angiotensin-converting enzyme 2 inhibits apoptosis of pulmonary endothelial cells during acute lung injury through suppressing MiR-4262. Cell Physiol Biochem 37:759–767. https://doi.org/10.1159/000430393.
34. Ji Y, Gao F, Sun B, Hao J, Liu Z. 2015. Angiotensin-converting enzyme 2 inhibits apoptosis of pulmonary endothelial cells during acute lung injury through suppressing SMAD2 phosphorylation. Cell Physiol Biochem 35:2203–2212. https://doi.org/10.1159/000374025.
35. Li Y, Cao Y, Zeng Z, Liang M, Xue Y, Xi C, Zhou M, Jiang W. 2015. Angiotensin-converting enzyme 2/angiotensin-(1–7)/Mas axis prevents lipopolysaccharide-induced apoptosis of pulmonary microvascular endothelial cells by inhibiting JNK/NF-κB pathways. Sci Rep 5:8209. https://doi.org/10.1038/srep08209.
36. Karlsson QH, Schelcher C, Verrall E, Petosa C, Sinclair AJ. 2008. Methylated DNA recognition during the reversal of epigenetic silencing is regulated by cysteine and serine residues in the Epstein-Barr virus lytic switch protein. PLoS Pathog 4:e1000005. https://doi.org/10.1371/journal.ppat.1000005.
37. Lieberman PM. 2015. Chromatin structure of Epstein-Barr virus latent episomes. Curr Top Microbiol Immunol 390:71–102. https://doi.org/10.1007/978-3-319-22822-8_5.
38. Bunyavanich S, Do A, Vicencio A. 2020. Nasal gene expression of angiotensin-converting enzyme 2 in children and adults. JAMA 323:2427–2429. https://doi.org/10.1001/jama.2020.8707.
39. Hadinoto V, Shapiro M, Sun CC, Thorley-Lawson DA. 2009. The dynamics of EBV shedding implicate a central role for epithelial cells in amplifying viral output. PLoS Pathog 5:e1000496. https://doi.org/10.1371/journal.ppat.1000496.
40. Pegtel DM, Middeldorp J, Thorley-Lawson DA. 2004. Epstein-Barr virus infection in ex vivo tonsil epithelial cell cultures of asymptomatic carriers. J Virol 78:12613–12624. https://doi.org/10.1128/JVI.78.22.12613-12624.2004.
41. Ling PD, Lednicky JA, Keitel WA, Poston DG, White ZS, Peng R, Liu Z, Mehta SK, Pierson DL, Rooney CM, Vilchez RA, Smith EO, Butel JS. 2003. The dynamics of herpesvirus and polyomavirus reactivation and shedding in healthy adults: a 14-month longitudinal study. J Infect Dis 187:1571–1580. https://doi.org/10.1086/374739.
42. Eichelberg MR, Welch R, Guidry JT, Ali A, Ohashi M, Makielski KR, McChesney K, Van Sciver N, Lambert PF, Keleș S, Kenney SC, Scott RS, Johannsen E. 2019. Epstein-Barr virus infection promotes epithelial cell growth by attenuating differentiation-dependent exit from the cell cycle. mBio 10:e01332-19. https://doi.org/10.1128/mBio.01332-19.
43. Verma D, Kim EA, Swaminathan S. 2013. Cell-based screening assay for antiviral compounds targeting the ability of herpesvirus posttranscriptional regulatory proteins to stabilize viral mRNAs. J Virol 87:10742–10751. https://doi.org/10.1128/JVI.01644-13.
44. Verma D, Ling C, Johannsen E, Nagaraja T, Swaminathan S. 2009. Negative autoregulation of Epstein-Barr virus (EBV) replicative gene expression by EBV SM protein. J Virol 83:8041–8050. https://doi.org/10.1128/JVI.00382-09.